Food Chemistry: X 24 (2024) 101958

Contents lists available at ScienceDirect

Food Chemistry: X

journal homepage: www.sciencedirect.com/journal/food-chemistry-x

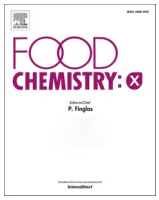

Design and fabrication of self-calibration colorimetric/fluorescence/SERS tri-modal optical sensor for highly rapid and accurate detection of mercury ions in foods

Jinxin Chen [a], Cheng Zhang [a], Lunzhao Yi [a], Fengmin Duan [b], Ying Gu [a], Kun Ge [a,*], Xuejing Fan [a,*]

[a] Faculty of Food Science and Engineering, Kunming University of Science and Technology, Kunming, 650500, China
[b] YunNan Institute of Measuring and Testing Technology, Kunming 650228, China

ARTICLE INFO

Keywords:
Tri-modal optical sensors
Self-calibration
Aminated rhodamine 6G
Hg^{2+}
Food safety

ABSTRACT

The improvement of detection accuracy without loss of rapidity and sensitivity by optical sensors in complex food analysis is still full of challenges owing to the matrix interference. Herein, a novel and simple self-calibration colorimetric/fluorescence/surface-enhanced Raman spectroscopy (SERS) tri-modal optical sensor based on aminated Rhodamine 6G (R6G-NH_2) was developed for highly rapid, sensitive, and accurate detection of Hg^{2+} in food samples. The high recognition specificity of R6G-NH_2 for Hg^{2+} can be achieved through the metal chelation interaction between Hg^{2+} and -NH_2, -COOH groups in R6G-NH_2 with formation of R6G-NH_2-Hg^{2+}-R6G-NH_2 complex. The DFT and FDTD simulations were adopted to confirm the theoretical feasibility in Hg^{2+} detection by tri-modal optical. Under the optimum conditions, the analytical method based on self-calibration tri-modal optical sensor for Hg^{2+} detection was established with promising properties (rapidity, linearity, linear range, LOD, and LOQ), providing a strategy in rapid, selective, sensitive, and accurate detection for food safety.

1. Introduction

With the rapid development of economy and society, and the significant improvement of living standard, several focal issues have been beginning to emerge. Among these issues, food safety issues associated with existent hazards in foods have drawn increasing concern due to their potential risks to human health (Su et al., 2024; Yi et al., 2024). It is well known that the determination of hazards content in foods is the prerequisite for food safety control. Thus, various analytical methods including traditional chromatography (Cacciola et al., 2020; Rocío-Bautista et al., 2022), electrochemical method (Gu et al., 2020), spectrometry (Kun Ge et al., 2023; K. Ge et al., 2019), enzyme linked immunosorbent assay (ELISA) (Civera et al., 2024), and atomic spectrum (Song et al., 2023), have been established to monitor food hazards for ensuring the food quality and safety. Among these methods, spectroscopy has been considered as the efficient methods owing to their advantages of rapidity, portability, and sensitivity in food safety analysis (Deepa & Ganesh, 2016; Peveler, 2024). Various spectroscopic methods have been adopted for high analysis of food contaminants, such as ultraviolet-visible (UV–Vis) spectroscopy (Tsotsou & Potiriadi, 2022), and fluorescence spectroscopy (Tang et al., 2022), and surface-enhanced Raman spectroscopy (SERS) (Neng et al., 2020). However, the low detection accuracy induced by instability and irreversibility of general optical sensors still limit their practicality and reliability in high-quality detection, especially in complex food samples (Fang et al., 2021).

Currently, several sample pre-treatment methods are considered as the effective tool to reduce the matrix interference and improve the detection accuracy, such as liquid−liquid extraction (Marsousi et al., 2019), headspace microextraction (Zhu et al., 2024), magnetic extraction (Mhd Haniffa et al., 2021), and solid phase micro extraction (SPME) (Yang et al., 2023). However, the complex operation and long proceeding time of sample pre-treatment method still need be improved (Chen et al., 2017). In addition, combining the features of different spectroscopic instruments can identify and correct errors caused by system itself or during the detection process, ensuring accurate and reliable results (L. Yang, et al., 2024; H. Zhang, Li, et al., 2022). For instance, when rapid detection of a large number of actual samples, a portable spectrometer can be used for initial screening (Piotrowski et al.,

* Corresponding authors.
E-mail addresses: Gekun@kust.edu.cn (K. Ge), fanxuejing@kust.edu.cn (X. Fan).

https://doi.org/10.1016/j.fochx.2024.101958
Received 28 September 2024; Received in revised form 20 October 2024; Accepted 31 October 2024
Available online 1 November 2024

2019), followed by more accurate quantitative analysis by one or more spectroscopy (Wang et al., 2023), namely self-calibration strategy. Zhang et al. (Hanqiang Zhang et al., 2023) proposed a colorimetric/fluorescence dual-model sensors based on thymine-modified Au nanoparticles/reduced-state sulfur nanodots (T-AuNPs/r-SDs) for highly accurate determination of Hg^{2+} through mutual calibration. Additionally, Au nano bipyramids-persistent luminescence nanoparticle composites (Au NBPs-ZGGO NP) were designed and fabricated for fluorescence/SERS dual-model analysis of *Staphylococcus aureus* enterotoxins (Zhao et al., 2021). The high detection accuracy can be achieved via self-calibration between fluorescence and SERS method. Thus, the multi-modal optical sensor is a promising candidate for accuracy enhancing in detection of food hazards in complex samples (Sun et al., 2023).

Heavy metal ions are one of the major risk factor to human health through foulants of water, soil, and air (Meng et al., 2023). Among various heavy metal ions, mercury ion (Hg^{2+}) (even low levels) show irreversible damages to human health, particularly affecting the nervous system, kidneys, and liver (Zamora-Ledezma et al., 2021). In addition, Hg^{2+} can bioaccumulate through the food chains including water, fruits, meat, vegetables, and grains (Hernández-Martínez & Navarro-Blasco, 2013; Song et al., 2023). The safety value of Hg^{2+} ions in drinking water are set to 6.0 μg/L by the World Health Organization (WHO), suggesting the rapid, sensitive, and accurate analytical methods for Hg^{2+} detection is essentially urgent (Gu et al., 2021; Luo et al., 2022). Currently, the combination of optical sensors with probe molecules in detection of heavy metal ions has gradually received considerable attentions (Kumar, 2023; Nan et al., 2021; Zhang, Zhong, et al., 2022). The specific reaction between heavy metal ions and functional groups of probe molecules generally exhibit higher sensitivity and selectivity, mainly caused by significant structural changes of probe molecules (Fan et al., 2022). For example, it has been reported that the core shell magnetite colloid nanocrystal clusters-poly methacrylic acid magnetic beads coupled with aptamers have been developed to detect Hg^{2+} using fluorescence/SERS dual-modal sensor (Li et al., 2020). Lan et al. (Lan et al., 2018) prepared a fluorescent probe based on pyrazole derivatives modifying rhodamine for UV–Vis/fluorescence dual-modal analysis of Hg^{2+} with high selectivity and accuracy. Thus, the development of probe molecules with multi-modal optical sensors is an ideal strategy for highly rapid, sensitive, selective, and accurate detection of Hg^{2+}.

In the present work, we proposed a novel self-calibration colorimetric/fluorescence/SERS tri-modal optical sensor based on aminated Rhodamine 6G (R6G-NH_2) probe for highly rapid, sensitive, and accurate detection of Hg^{2+} in food samples. The -NH_2 and -COOH groups in R6G-NH_2 can interact with Hg^{2+} with high specificity to form R6G-NH_2-Hg^{2+}-R6G-NH_2 complex through metal chelation reaction, thus inducing optical changes in UV–Vis, fluorescence, and SERS spectrum. In addition, the theoretical feasibility in Hg^{2+} detection by self-calibration tri-modal optical sensor was validated by DFT and FDTD calculations. The rapidity (within 13 min) and high accuracy (through self-calibration function) for detection of Hg^{2+} can be achieved using tri-modal optical sensor. Under the optimum conditions, the detection method for Hg^{2+} based on self-calibration tri-modal optical sensor was established with promising analytical performance (linearity, linear range, LOD, and LOQ). Finally, the as-developed method based on tri-modal optical sensor was applied to determination of Hg^{2+} in real food samples, showing great superiorities in recoveries, RSDs, and accuracy (self-calibration function). The established method provides a new venue in quantitative detection of hazards in complex food samples with high rapidity, selectivity, sensitivity, and accuracy by multi-modal optical sensors with self-calibration function.

2. Experimental section

2.1. Chemicals and reagents

All used chemicals and reagents were at least analytically pure without further purification. Gold chloride trihydrate ($HAuCl_4{\cdot}3H_2O$, 99.9 %) was purchased from Bide Pharmatech Co., Ltd. (Shanghai, China). Rhodamine 6G (R6G, 95 %), ethylenediamine (EDA, 98 %) and anhydrous sodium citrate ($C_6H_5O_7Na_3$, 99 %) were obtained from Aladdin Biochemistry Science and Technology Co., Ltd. (Shanghai, China). Mercury ion standard solution (Hg^{2+}, 1.0 mg/mL) was provided by Sinopharm Chemical Reagent Co., Ltd. (Tianjin, China). Methanol (MeOH, 99.9 %), acetonitrile (ACN, 99.9 %), anhydrous ethanol (EtOH, 99.7 %), and trichloroacetic acid (TCA, 99.5 %) were obtained from Shanghai Macklin Biochemical Technology Co., Ltd. (Shanghai, China). Ultrapure water with resistivity of 18.2 MΩ/cm was used for all experiments and the glassware was cleaned using aqua regia (HCl: HNO_3 = 3:1, *v/v*) before used. The other chemicals and regents can be seen S1 in Supplementary Materials.

2.2. Instruments

The UV–Vis, fluorescence and SERS analysis was recorded by Shimadzu UV-2600i spectrophotometer (Shimadzu, Japan), F-4600 fluorescence spectrophotometer (Hitachi, Japan), and i-Raman Plus portable Raman spectrometer (λ_{ex} = 785 nm, BWTek, USA), respectively. The characterizations of AuNPs was conducted by JEM-2100 transmission electron microscope (TEM, JEOL, Japan) and Zetasizer Nano ZS90X DLS (Malvern, UK), respectively. The R6G-NH_2 probe was characterized by LC-MS-IT-TOF HRMS (Shimadzu, Japan), INVENIO-S FTIR (Fourier transfer infrared, FT-IR, Bruker, UK) and x-ray photoelectron spectroscopy (XPS, Thermo Scientific K-Alpha, UK), respectively. HZP-T503 PH Meter (Huazhi, China) was used to monitoring the pH value. The concentration of Hg^{2+} was confirmed by inductively coupled plasma mass spectrometry (ICP-MS, Agilent 5800, US).

2.3. Synthesis of R6G-NH_2 probe

Generally, the R6G-NH_2 probe with spirolactam-closed structure was prepared according to previous methods (P. Li et al., 2013). The detailed preparation process was described as follows: 4.0 mmol of R6G was rapidly dissolved in hot EtOH (40 mL), followed by injection of EDA (1.4 mL). Then, the resulting mixture was refluxed at 85 °C for several hours until the color of mixture was changed to light pink. After cooling down to room temperature, the precipitate was washed with cold EtOH (60 mL) for three times. Finally, the result product was recrystallized by cold ACN to obtain pure R6G-NH_2 powder (white–pink color).

2.4. Detection of Hg^{2+} by tri-modal optical sensor

The self-calibration colorimetric/fluorescence/SERS tri-modal optical sensor was applied to detection of Hg^{2+} in standard solution to investigate the analytical performance of method. Generally, 8.0 mg/L R6G-NH_2 (1.0 mL) was mixed with different concentrations of Hg^{2+} standard solution (1.0 mL), followed by incubation at room temperature (25 °C) for 8 min to obtain the reaction mixture. For colorimetric and fluorescence detection, UV–vis absorption at 529 nm and fluorescence emission intensity at 556 nm (Ex = 530 nm) were recorded. For SERS analysis, the enhanced substrate of Au nanoparticles (AuNPs) was prepared (Please see S2 in Supplementary Materials). Thus, 0.15 mL obtained reaction mixture was mixed with 0.15 mL concentrated AuNPs in 96-pore plate for 5 min, followed by SERS detection. The SERS detection parameters are present as follows: wavelength range: 200–2000 cm^{-1}; integral time: 5 s; laser power: 210 mW. All optical measurement (colorimetric/fluorescence/SERS) was repeated three times with parallel three samples.

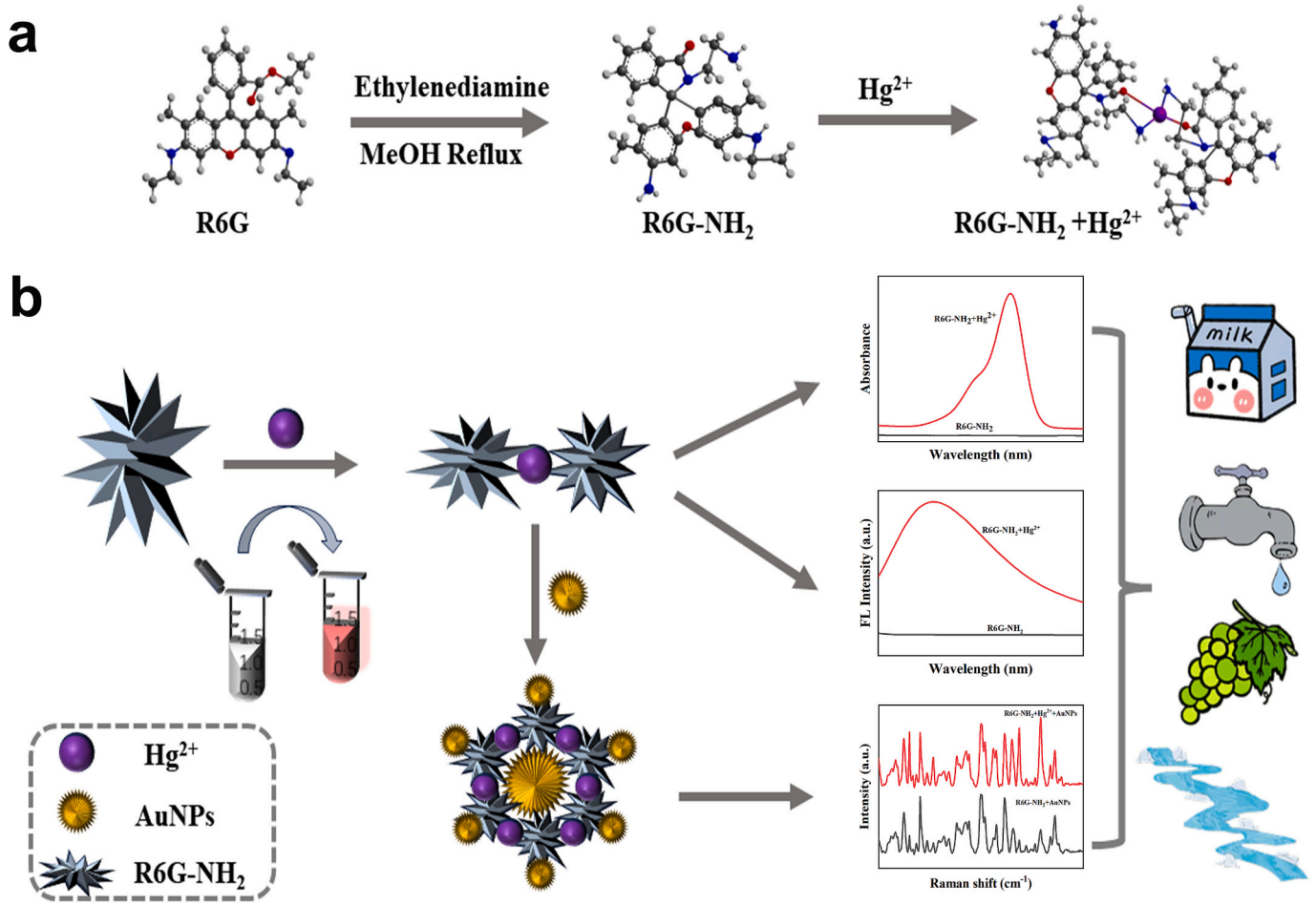

Scheme 1. Schematic illustration of preparation of R6G-NH_2 probe for self-calibration colorimetric/fluorescence/SERS tri-model optical analysis of Hg^{2+} in foods.

2.5. Analysis of Hg^{2+} in actual sample

The as-developed self-calibration colorimetric/fluorescence/SERS tri-modal optical sensor was applied to detection of Hg^{2+} in real samples to confirm the feasibility of method. Four kinds of food samples including skimmed milk and grapes (from local supermarket in Kunming), tap water (from a laboratory in Kunming) and river water (from Laoyu River in Kunming) were used as actual samples. Before the tri-modal detection, the essential sample pre-treatment process was adopted for reducing the matrix interference. The purchased skimmed milk (2.5 mL) was treated with 1.0 mL trichloroacetic acid (30 %, *v/v*) by vortexing for 5 min to remove proteins. Then, the result mixture was centrifuged at 10,000 rpm for 15 min, and the supernatant was collected and filtered by 0.22 μm nylon membrane. The collected tap water and river water were centrifuged at 11,000 rpm for 30 min, and the supernatant was collected and filtered by 0.22 μm nylon membrane. Grapes were firstly juiced, followed by been mixed with ultrapure water. The result mixture was centrifuged at 10,000 rpm for 20 min, and the supernatant was collected and filtered by 0.22 μm nylon membrane. After sample pre-treatment process, the concentration of Hg^{2+} in above actual samples were measured by self-calibration tri-modal analysis with similar process with standard solution of Hg^{2+}. The standard ICP-MS method was also used to further evaluate the accuracy of tri-modal optical method.

3. Results and discussion

3.1. Preparation and characterization of R6G-NH_2 probe

The R6G-NH_2 probe with high specificity for Hg^{2+} was prepared by spirolactam-closed R6G based on Michael addition reaction (Scheme 1a). The functional groups with high chemical affinity provide dominant position for recognition of Hg^{2+} with selectivity, exhibiting tri-modal signals including UV–Vis absorption, fluorescence, and SERS spectra (Scheme 1b). On the one hand, the rapid and selective analysis of Hg^{2+} can be achieved based on the quick response of optical sensing and high specificity of R6G-NH_2 probe for Hg^{2+}. On the other hand, the self-calibration functions with colorimetric/fluorescence/SERS tri-modal optical sensor ensure the high detection accuracy.

The fluorescence emission, UV–visible absorption, and SERS spectra were investigated to compare differences between R6G and R6G-NH_2. It can be found that the R6G-NH_2 exhibited negligible peak (fluorescence emission and UV–visible absorption spectra) compared with R6G (Fig. S1a, b), and the SERS spectra intensity shows opposite phenomenon (Fig. S1c). The excitation (Ex) and emission (Em) spectra of R6G-NH_2 illustrated the Ex and Em peak at 530 and 556 nm, respectively (Fig. S1d). In addition, the ESI-HRMS, FT-IR and XPS analysis were adopted to confirm the successful preparation of R6G-NH_2. In addition, the R6G-NH_2 molecule was characterized using ESI-HRMS with mass-to-charge ratio (*m/z*) of 457.2, suggesting the successful preparation of R6G-NH_2 by R6G (Fig. S1e). The FT-IR spectra was performed on R6G-NH_2 and R6G powder to further verify the successful synthesis of R6G-NH_2. As it can be seen in Fig. S1f, the R6G-NH_2 displayed stretching vibration at 1685 cm^{-1}, corresponding to the formation of amide

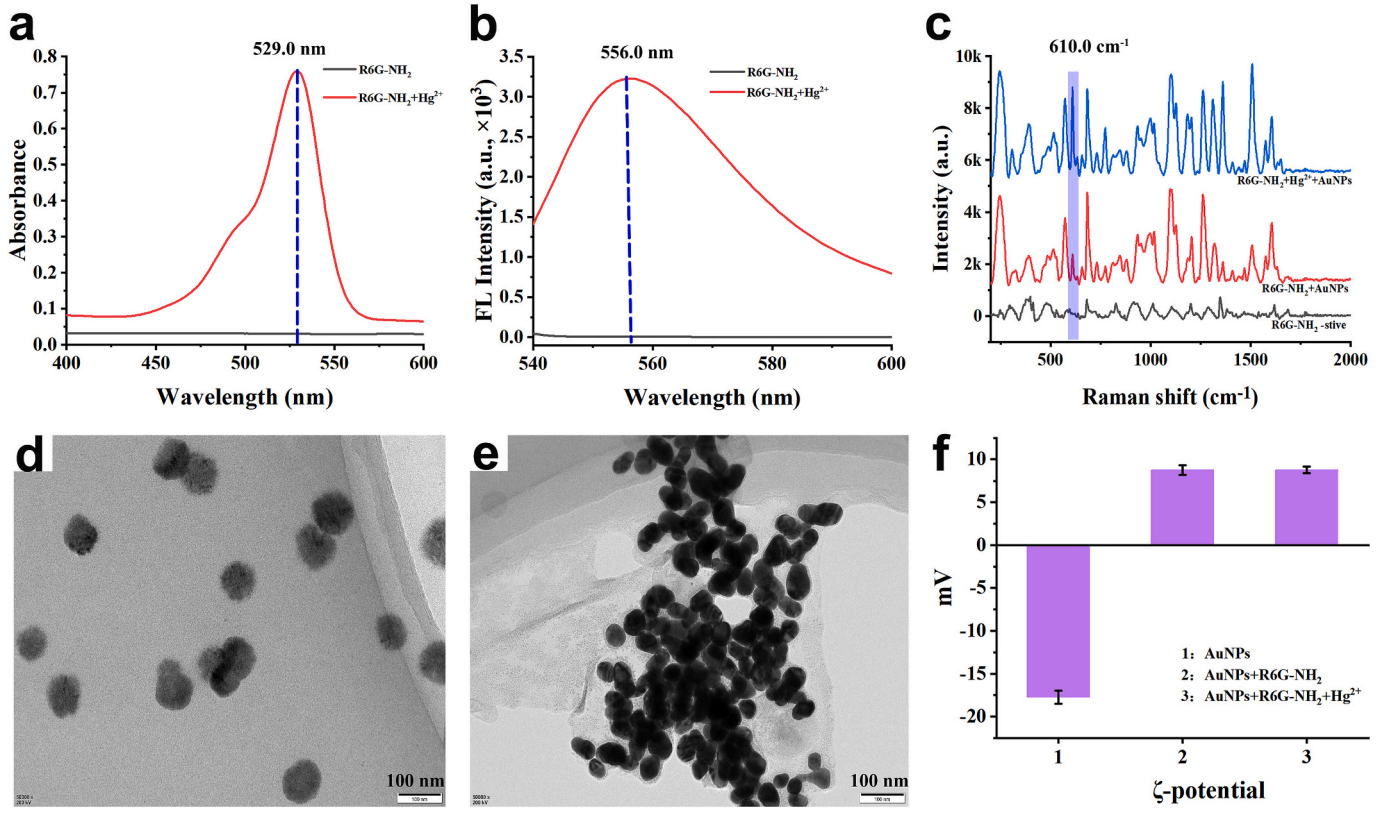

Fig. 1. The feasibility of colorimetric (a), fluorescence (b), and SERS (c) analysis of Hg^{2+} by R6G-NH_2 probe. TEM images for AuNPs (d) and R6G-NH_2 + AuNPs + Hg^{2+} (e). Zeta potential for AuNPs, R6G-NH_2 + AuNPs, and R6G-NH_2 + AuNPs + Hg^{2+}.

structure (-C=O) from the reaction between carboxyl group (-COO) of R6G (1715 cm^{-1}) and ethylenediamine (EDA). Furthermore, the obvious peaks at 2930 and 2967 cm^{-1} were attributed to the asymmetric and symmetric stretching vibrations of the -CH_2CH_2- group. Finally, the most prominent two FT-IR characteristic peaks above 3300 cm^{-1}, corresponding to the free -NH_2 groups, providing further confirmation of successful formation of R6G-NH_2. Additionally, the XPS analysis was performed on R6G-NH_2 and R6G powder to further verify the successful preparation of R6G-NH_2. As it can be seen in Fig. S2, the same elemental composition (C, N, O) for R6G-NH_2 and R6G was observed. As shown in Fig. S3a, the XPS spectra of C 1 s for R6G exhibits peaks at 283.3 eV, 284.9 eV, and 287.6 eV, attributing to C-C/C=C, C-O/C-N, and O-C=O, respectively. For R6G-NH_2, the obvious peaks at 283.7 eV, 284.8 eV, and 285.5 eV assigned to C-C/C=C, C-O/C-N, and C=O indicated the transformation of R6G (O-C=O bond, 287.6 eV) to R6G-NH_2 (C=O bond, 285.5 eV) (Fig. S3d). Fig. S3b shows the detailed N 1 s peak of R6G at 397.9 eV and 398.8 eV, corresponding to N—H and -N=, respectively. After converting to R6G-NH_2, the detailed XPS peaks at 396.6 eV (C—N (—C, —R)), 397.8 eV (N—H), and 398.6 eV (—NH_2) can be confirmed (Fig. S3e). The obvious change of detailed XPS spectra (N 1 s) can be attributed to the reaction between R6G and ethylenediamine. The detailed O 1 s peaks at 530.5 eV and 530.9 eV represent the formation of C=O and C—O bond in both R6G and R6G-NH_2 (Fig. S3c, f). These above XPS results demonstrate that R6G-NH_2 was successfully prepared based on R6G.

3.2. The feasibility of tri-modal optical sensor

Considering the high specificity of R6G-NH_2 for Hg^{2+}, we propose a self-calibration colorimetric/fluorescence/SERS tri-modal optical method for highly rapid and accurate analysis of Hg^{2+} based on metal chelation reaction. R6G-NH_2 has an aminated ring-closed spirocyclic structure based on the parent of the R6G-based xanthine, indicating the formation of R6G-NH_2-Hg^{2+}-R6G-NH_2 complex through strong coordination with metal ions by amino (-NH_2) and carboxyl (-COOH) groups (P. Li et al., 2013). The color of R6G-NH_2 will be changed from colorless to light pink after addition Hg^{2+} (Fig. S4), leading to optical changes in colorimetric, fluorescence, and SERS. As shown in Fig. 1a–c, the UV–Vis absorption (529 nm), fluorescence intensity (556 nm), and SERS intensity (610 cm^{-1}) significantly increased after addition of Hg^{2+} (100.0 μg/L), suggesting the feasibility in selective detection of Hg^{2+} by R6G-NH_2 probe. In addition, the characterizations of AuNPs in TEM, Zeta potential, and dynamic light scattering (DLS) were further performed to verify the feasibility. As displayed in Fig. 1d, e, the AuNPs showed aggregation after addition of Hg^{2+} in the presence of R6G-NH_2 probe. The AuNPs with negative charge will interact with positively charged R6G-NH_2 molecules, leading to the observed aggregation (Fig. 1f). Finally, the size distribution of AuNPs significantly increased from 43 nm to 459 nm in the presence of R6G-NH_2 probe and Hg^{2+} (Fig. S5).

In addition, the simulations based on density functional theory (DFT) and finite difference time domain (FDTD) were adopted to further confirm the feasibility. As it can be seen in Fig. S6, the Gibbs free energy (Δ_G) for recognition of Hg^{2+} by R6G-NH_2 probe was −4.4 eV, meaning the high specificity of R6G-NH_2 for Hg^{2+}. Additionally, the electromagnetic field distribution of AuNPs was investigated by FDTD simulations (Fig. S7). The strongest electromagnetic field intensity can be found when the distance between AuNPs is 0.5 nm and the electromagnetic field intensity was significantly decreased with distance increased, demonstrating the strong correlation between distance of AuNPs and electromagnetic field intensity. Thus, the feasibility of SERS detection of Hg^{2+} by R6G-NH_2 probe further can be confirmed based on AuNP aggregation. The above results suggest the high feasibility of R6G-NH_2 probe for highly rapid and selective analysis of Hg^{2+}.

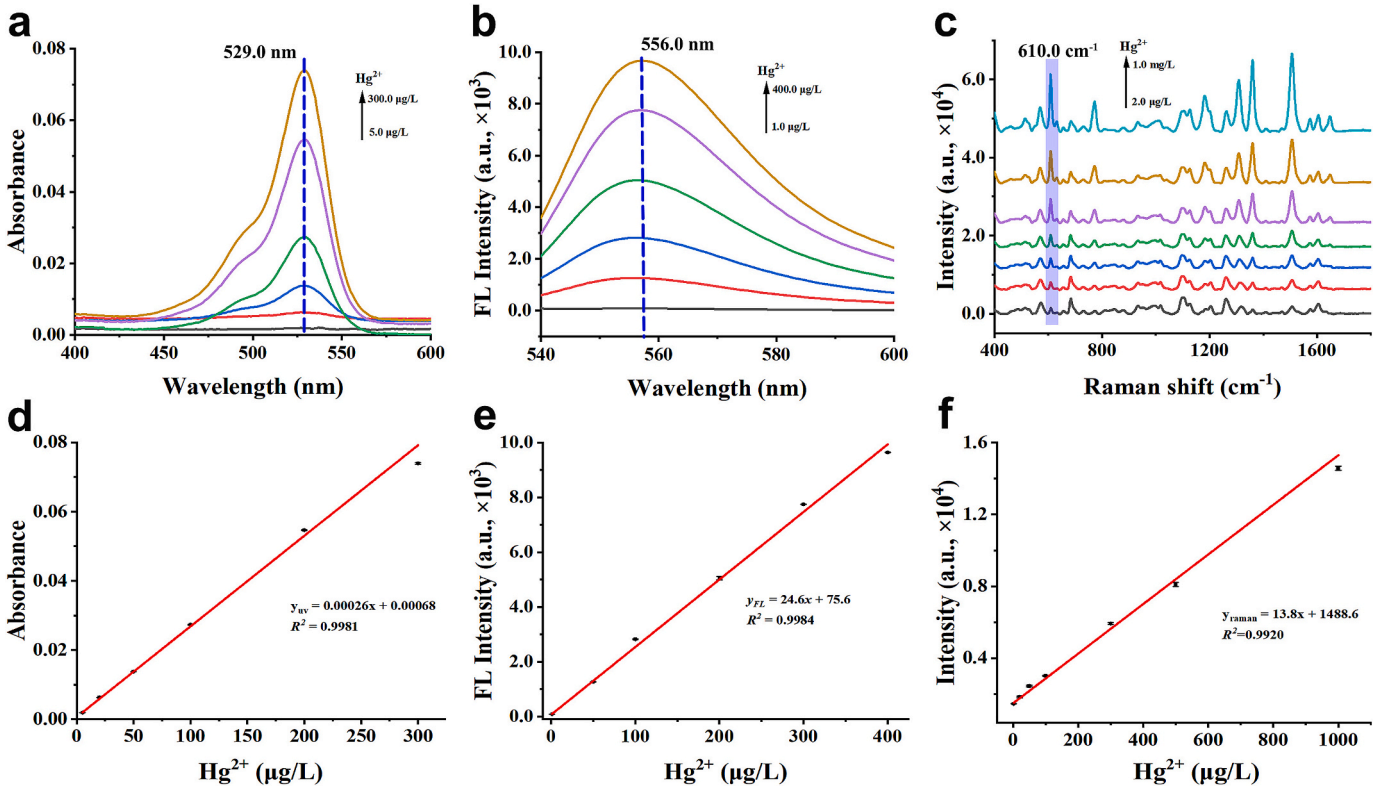

Fig. 2. The UV-Vis (a), fluorescence (b), and SERS (c) intensity of Hg^{2+} at different concentration. Plot of UV-Vis absorption (d), fluorescence emission intensity (e), and SERS intensity (f) against Hg^{2+} concentration with the linear range from 5.0 to 300.0 μg/L, 1.0 to 400.0 μg/L, and 2.0 to 1000.0 μg/L, respectively.

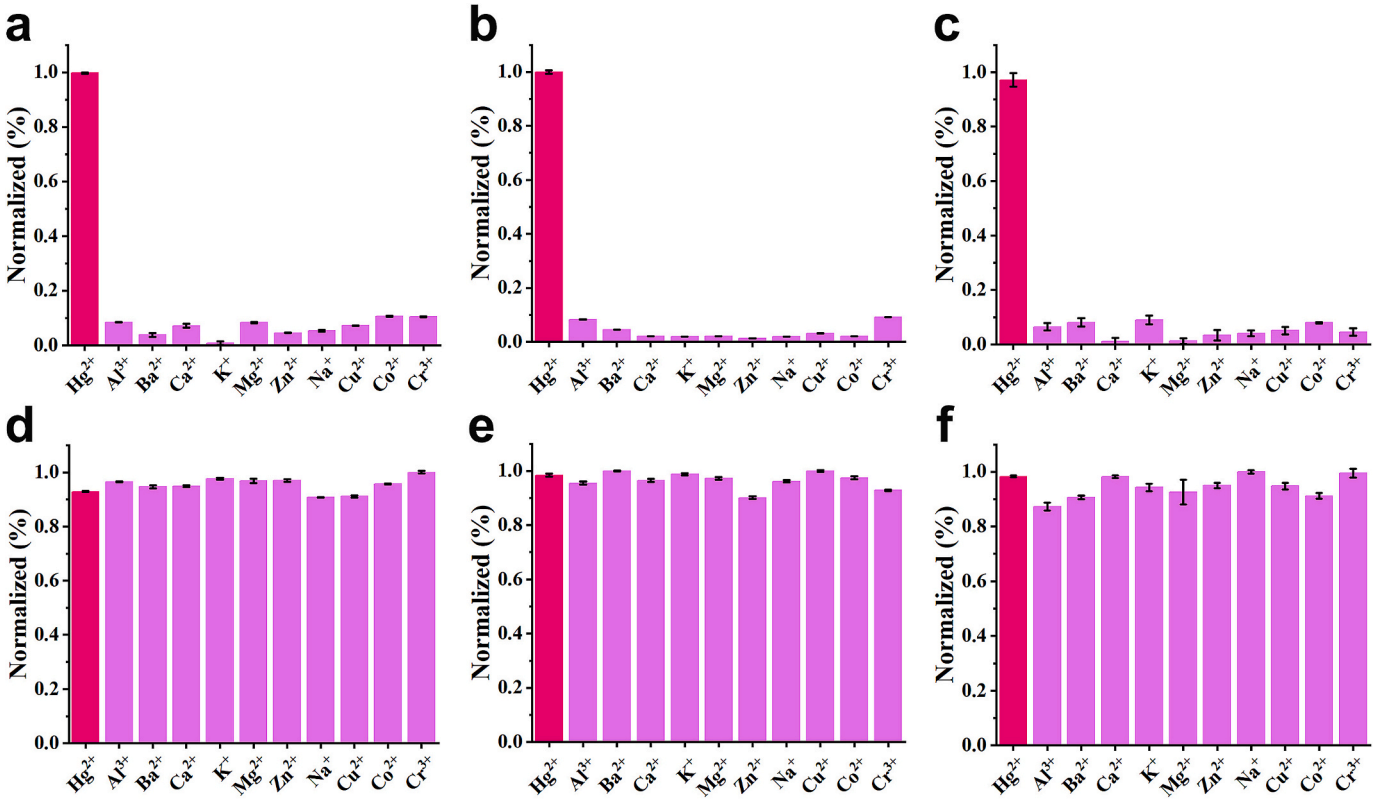

Fig. 3. Selectivity of colorimetric/fluorescence/SERS tri-modal optical sensor for 100.0 μg/L Hg^{2+} over other interfering metal ions by colorimetric (a), fluorescence (b), and SERS (c) method. Anti-interference ability of colorimetric/fluorescence/SERS tri-modal optical sensor for 100.0 μg/L Hg^{2+} over other interfering substance by colorimetric (d), fluorescence (e), and SERS (f) method.

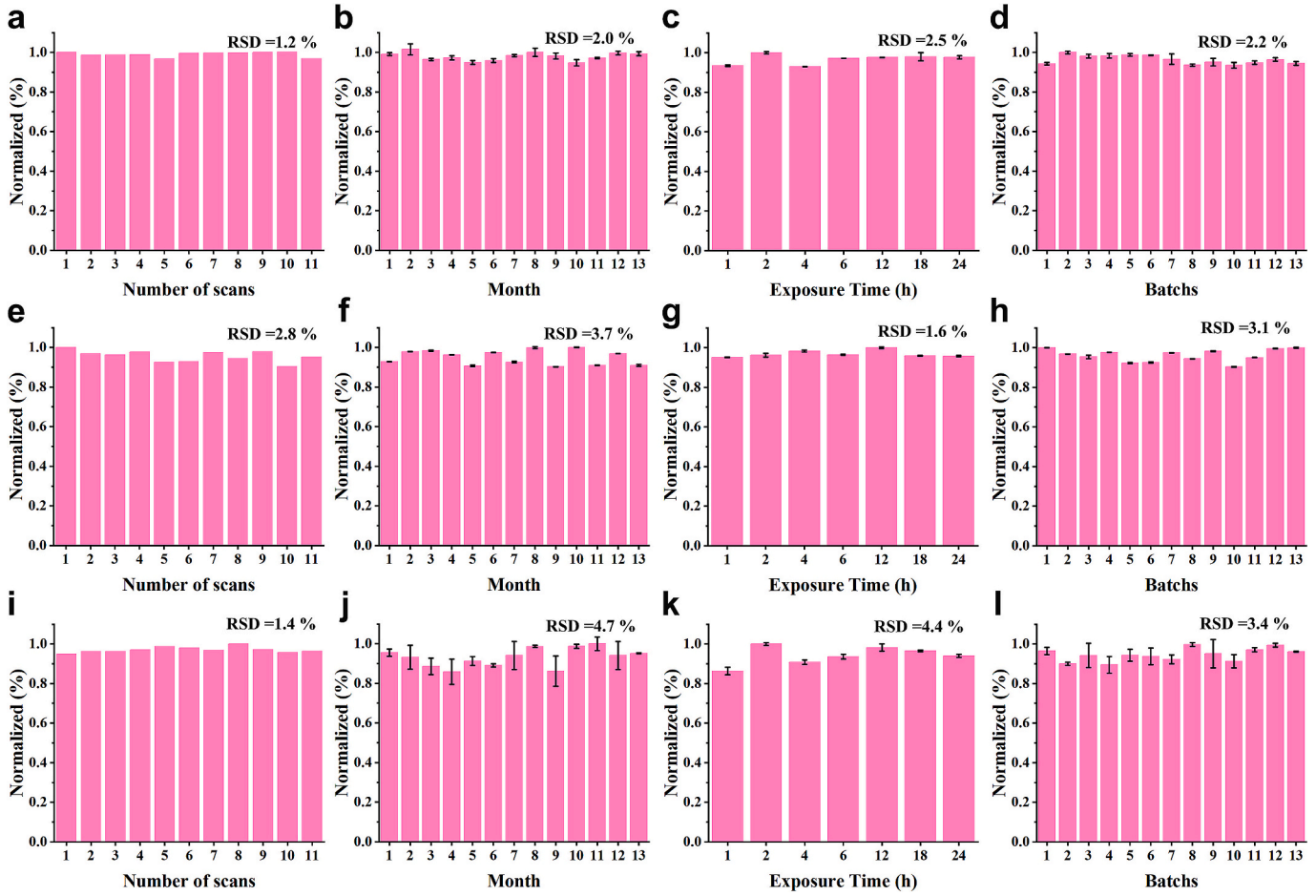

Fig. 4. Stability of colorimetric/fluorescence/SERS tri-modal optical sensor for detecting 100.0 μg/L Hg^{2+} in 11 replicates (a, e, i), 13 consecutive months (b, f, j), 24 consecutive exposure hours (c, g, k), and 13 different batches (d, h, l) by colorimetric (a–d), fluorescence (e–h), and SERS (i–l) method.

3.3. Optimization of tri-modal optical method

Before the quantitative detection of Hg^{2+}, several experiment parameters including pH value, concentration of R6G-NH_2 probe, and reaction time of have been investigated to obtain the best detection performance. The effects of pH value with different buffer solutions on UV–Vis absorption, fluorescence emission intensity, and SERS intensity in the presence of R6G-NH_2 were evaluated. As shown in Fig. S8, the UV–Vis absorption, fluorescence intensity, and SERS intensity of R6G-NH_2 exhibited unstable signals in pH range from 1.0 to 11.0 with three common buffers including PBS, HAc-NaAc, and Tris-HCl buffer. The above results suggest the pH sensitivity of R6G-NH_2 probe, demonstrating that the ultrapure water was best solvent for next detection process. Furthermore, the concentration of R6G-NH_2 probe is a crucial factor in affecting sensitivity and selectivity for Hg^{2+} determination. As it can be seen in Fig. S9, R6G-NH_2 probe with different concentration (0–12.0 mg/L) yielded different UV–Vis absorbance, fluorescence emission intensity, and Raman intensity at 529 nm, 556 nm and 610 cm^{-1}, respectively. The UV–Vis absorbance, fluorescence emission intensity, and Raman intensity increased as the heating concentration increased from 0 to 12.0 mg/L, and then shows downward trend. Finally, the incubation time between R6G-NH_2 probe and Hg^{2+} was optimized. As displayed in Fig. S10a, b, the UV–Vis absorbance and fluorescence emission intensity got the highest signal in incubation time of 8 min. For further SERS analysis, the best incubation time between mixture of R6G-NH_2 probe + Hg^{2+} and AuNPs was also obtained in 5 min, which exhibited highest SERS intensity at 610 cm^{-1} (Fig. S10c).

3.4. Development of tri-modal optical sensor for analysis of Hg^{2+}

Under the optimum conditions, the optical response of tri-modal optical sensor to Hg^{2+} with different concentrations was investigated and the fitting standard curve was further established. As shown in Fig. 2a–c, the UV–Vis absorption (529 nm), fluorescence emission (556 nm), and SERS intensity (610 cm^{-1}) gradually increased with the increase of concentration of Hg^{2+} in range of 5.0–300.0, 1.0–400.0, and 2.0–1000.0 μg/L, respectively. The fitting relationship between the spectral intensity and the concentrations of Hg^{2+} was plotted with correlation coefficient (R^2) of 0.9981, 0.9984, and 0.9920 for UV–Vis, fluorescence, and SERS model, respectively (Fig. 2d–f). The linear equation of $y_{UV-Vis} = 0.00026\times + 0.00068$, $y_{FL} = 24.6\times + 75.6$, and $y_{SERS} = 13.8\times + 1488.6$ can be obtained for above optical models. The LOD and LOQ for UV–Vis, fluorescence, and SERS model were 1.5 and 5.1 μg/L, 1.2 and 4.1 μg/L, 1.8 and 5.9 μg/L, respectively. Hence, the recognition of Hg^{2+} by self-calibration colorimetric/fluorescence/SERS tri-modal optical sensor exhibited high rapidity, sensitivity, and consistency, making it suitable for the quantitative detection of Hg^{2+} in food samples.

The selectivity and anti-interference ability of self-calibration tri-modal optical sensor was evaluated before next actual sample analysis. Fig. 3a–c exhibited that the Al^{3+}, Ba^{2+}, Ca^{2+}, K^{+}, Mg^{2+}, Zn^{2+}, Na^{+}, Cu^{2+}, Co^{2+}, and Cr^{3+} with different folds (please see Table S1) have negligible optical response on tri-modal sensor including UV–Vis absorption, fluorescence emission intensity, and Raman intensity compared to Hg^{2+} (100.0 μg/L), meaning the good selectivity of tri-modal optical sensor for Hg^{2+} analogues. Moreover, the anti-

Table 1
Analysis of Hg^{2+} in foods with ICP-MS and colorimetric/fluorescence/SERS tri-modal optical method.

Samples	Original (ICP-MS)	Assay	Added (μg/L)	Found (μg/L)	Recovery (%)	RSD (%, n = 3)
Milk	N.D.[a]	UV	10.0	9.7	97.6	1.2
			50.0	49.9	99.7	0.6
			200.0	184.1	92.1	0.5
		FL	5.0	4.6	95.2	0.2
			50.0	47.9	96.1	0.2
			300.0	274.0	91.4	0.3
		SERS	5.0	9.9	104.5	2.1
			50.0	55.2	103.7	0.8
			500.0	435.8	89.2	0.9
Grape	N.D.	UV	10.0	10.4	102.9	1.9
			50.0	47.7	95.7	0.7
			200.0	195.1	97.6	1.3
		FL	5.0	3.9	86.7	0.6
			50.0	46.2	92.9	0.4
			300.0	310.0	103.3	0.1
		SERS	5.0	4.78	99.8	1.3
			50.0	47.2	98.1	0.7
			500.0	523.1	103.9	1.2
Tap water	N.D.	UV	10.0	9.4	95.1	1.7
			50.0	47.9	96.1	1.3
			200.0	187.9	94.0	0.7
		FL	5.0	3.8	84.6	0.5
			50.0	43.9	88.5	0.6
			300.0	307.0	102.3	0.1
		SERS	5.0	3.7	98.8	1.1
			50.0	46.8	97.8	2.7
			500.0	492.1	98.7	1.4
River water	N.D.	UV	10.0	9.7	97.9	2.6
			50.0	47.3	94.8	0.7
			200.0	191.6	95.9	1.3
		FL	5.0	3.8	85.1	0.4
			50.0	50.7	101.2	0.2
			300.0	293.3	97.8	0.1
		SERS	5.0	7.7	102.5	2.4
			50.0	50.8	100.6	2.0
			500.0	473.3	95.5	0.7

[a] N.D. = Not detected.

interference ability of self-calibration tri-modal optical sensor was further evaluated using above metal ions as interferences. As shown in Fig. 3d–f and Table S2, the above interfering metal ions show negligible effect on analysis of Hg^{2+} (100.0 μg/L) by tri-modal optical methods including UV–Vis absorption (529 nm), fluorescence emission intensity (556 nm), and Raman intensity (610 cm^{-1}). The above results demonstrate the practicality of tri-modal optical sensor in detection of Hg^{2+} in actual samples.

3.5. Stability and repeatability

The stability and repeatability of the self-calibration tri-modal optical sensor was evaluated for Hg^{2+} detection under various conditions. As shown in Fig. 4a, e, i, the detection of Hg^{2+} (100.0 μg/L) by tri-modal optical sensor for 11 repeat measurements exhibited low RSDs of 1.2 %, 2.8 %, and 1.4 % for colorimetric, fluorescence, and SERS model, respectively. In addition, the with long-term stability and repeatability of tri-modal optical sensor was evaluated within 13 months in the presence of Hg^{2+} (100.0 μg/L), displaying low RSDs of 2.0 %, 3.7 %, and 4.7 % for colorimetric, fluorescence, and SERS model, respectively (Fig. 4b, f, j). The good stability of tri-modal optical sensor also can be seen with exposure time in range of 1–24 h in the presence of 100.0 μg/L Hg^{2+} (RSDs ≤4.4 %) (Fig. 4c, g, k). Finally, the 13 batches of tri-modal optical sensors were applied to detection of Hg^{2+} (100.0 μg/L) with RSDs as low as 2.2 % (Fig. 4d, h, i), indicating the promising stability of inter-batch. The above results demonstrate the satisfied stability and repeatability of as-developed self-calibration tri-modal optical sensor for quantitative analysis of Hg^{2+}.

3.6. Analytical applications in food samples

To further validate the practicality and reliability of self-calibration tri-modal optical sensor, four food samples including skimmed milk, grapes, tap water, and river water were used as actual samples. The standard ICP-MS method was applied to confirm the detection accuracy of tri-modal optical sensor. As shown in Table 1, the Hg^{2+} can not be detected by using ICP-MS method, as well as colorimetric, fluorescence, and SERS tri-modal optical methods. Thus, certain concentrations of Hg^{2+} was spiked in food samples, known as recovery experiments. The recoveries of 92.1–102.9 %, 84.6–103.3 %, and 89.2–104.5 % can be found for colorimetric, fluorescence, and SERS method with RSDs of 0.5–2.6 %, 0.1–0.6 %, and 0.7–2.7 %, respectively (Table 1). In addition, relative errors within colorimetric, fluorescence, and SERS method was calculated to further confirm the detection accuracy and self-calibration function of tri-modal optical sensor. The difference of 6.0 %, 1.3 %, 3.7 %, and 3.3 % can be obtained for skimmed milk, grapes, tap water, and river water by colorimetric, fluorescence, and SERS model, respectively, indicating the high detection accuracy and self-calibration function of as-developed tri-modal optical sensor (Table S3). These results indicate that the self-calibration tri-modal optical sensor has great potential in rapid, accurate, and quantitative detection of Hg^{2+} for food samples with high reliability and accuracy, providing reliable analytical method for ensuring food safety.

4. Conclusion

In conclusion, a novel self-calibration colorimetric/fluorescence/SERS tri-modal optical sensor based on aminated Rhodamine 6G (R6G-NH_2) probe was designed and fabricated for highly rapid, sensitive, and accurate detection of Hg^{2+} in foods. The R6G-NH_2 with -NH_2 and -COOH groups will interact with Hg^{2+} for formation of R6G-NH_2-Hg^{2+}-R6G-NH_2 complex through metal chelation reaction, resulting in optical changes in UV–Vis, fluorescence, and SERS spectrum. Thus, the specific recognition and anti-interference properties of tri-modal optical sensor for Hg^{2+} can be confirmed. The theoretical feasibility of self-calibration tri-modal optical sensor was verified by DFT and FDTD simulations. In addition, the rapid and accurate detection for Hg^{2+} can be achieved within 13 min owing to the self-calibration function with tri-modal methods. Under the optimum conditions, the integration of tri-modal optical sensor enables promising analytical performance for Hg^{2+}, including broad detection range (1.0–1000.0 μg/L), good correlation coefficient (R^2 = 0.9981), low LOD (1.2 μg/L) and LOQ (4.1 μg/L). Finally, the self-calibration colorimetric/fluorescence/SERS tri-modal optical sensor was used to quantitative determination of Hg^{2+} in actual food samples, showing great superiorities in recoveries (84.6–104.5 %), RSDs (0.1–2.7 %), and accuracy (1.3–6.0 %, self-calibration tri-modal method). The tri-modal optical sensor was applied to analysis of Hg^{2+} in food samples, exhibiting excellent superiorities in recoveries and accuracy (self-calibration function). Our data opens a new venue in design and fabrication of multi-modal optical sensors with self-calibration function for detection of food hazards in complex food samples with high rapidity, selectivity, sensitivity, and accuracy.

CRediT authorship contribution statement

Jinxin Chen: Writing – original draft, Formal analysis, Data curation. **Cheng Zhang:** Formal analysis, Data curation. **Lunzhao Yi:** Formal analysis, Data curation. **Fengmin Duan:** Formal analysis. **Ying Gu:** Writing – review & editing. **Kun Ge:** Writing – review & editing, Writing – original draft, Supervision, Conceptualization. **Xuejing Fan:** Writing – review & editing, Supervision.

Declaration of competing interest

The authors declare that they have no known competing financial interests or personal relationships that could have appeared to influence the work reported in this paper.

Acknowledgements

This work was supported by the by the Yunnan Major Scientific and Technological Projects (Grant No. 202402AE090040) and Special Project for High-level Scientific and Technological Talents and Innovation Teams of Yunnan Province (Grant No. 202405AS350005).

Appendix A. Supplementary data

Supplementary data to this article can be found online at https://doi.org/10.1016/j.fochx.2024.101958.

Data availability

Data will be made available on request.

References

Cacciola, F., Rigano, F., Dugo, P., & Mondello, L. (2020). Comprehensive two-dimensional liquid chromatography as a powerful tool for the analysis of food and food products. *TrAC Trends in Analytical Chemistry, 127*, Article 115894. https://doi.org/10.1016/j.trac.2020.115894

Chen, Z., Li, G., & Zhang, Z. (2017). Miniaturized thermal-assisted purge-and-trap technique coupling with surface-enhanced Raman scattering for trace analysis of complex samples. *Analytical Chemistry, 89*(17), 9593–9600. https://doi.org/10.1021/acs.analchem.7b02912

Civera, A., Esteban, C., Mata, L., Sanchez, L., Galan-Malo, P., & Perez, M. D. (2024). Sensitive ELISA and lateral flow immunoassay for the detection of walnut traces in processed food and working surfaces. *Food Chemistry, 441*, Article 138296. https://doi.org/10.1016/j.foodchem.2023.138296

Deepa, N., & Ganesh, A. B. (2016). Design and development of portable opto-electronic sensing system for real-time monitoring of food fermentation. *Sensors and Actuators B: Chemical, 233*, 674–683. https://doi.org/10.1016/j.snb.2016.04.143

Fan, Q., Bao, G.-M., Li, S.-H., Liu, S.-Y., Cai, X.-R., Xia, Y.-F., Li, W., Wang, X.-Y., Deng, K., & Yuan, H.-Q. (2022). A dual-channel "on–off–on" fluorescent probe for the detection and discrimination of Fe^{3+} and Hg^{2+} in piggery feed and swine wastewater. *Analytical Methods, 14*(23), 2318–2328. https://doi.org/10.1039/d2ay00629d

Fang, L., Jia, M., Zhao, H., Kang, L., Shi, L., Zhou, L., & Kong, W. (2021). Molecularly imprinted polymer-based optical sensors for pesticides in foods: Recent advances and future trends. *Trends in Food Science & Technology, 116*, 387–404. https://doi.org/10.1016/j.tifs.2021.07.039

Ge, K., Hu, Y., & Li, G. (2023). Surface initiated encapsulation of MOF-74 (Ni) on magnetic prickly-like nickel rods combined with silver nanoparticle decoration for simultaneous and selective surface-enhanced Raman spectroscopy analysis of T-2 and deoxynivalenol. *Sensors and Actuators B: Chemical, 374*, Article 132842. https://doi.org/10.1016/j.snb.2022.132842

Ge, K., Liu, J., Wang, P., Fang, G., Zhang, D., & Wang, S. (2019). Near-infrared-emitting persistent luminescent nanoparticles modified with gold nanorods as multifunctional probes for detection of arsenic (III). *Microchimica Acta, 186*(3), 197. https://doi.org/10.1007/s00604-019-3294-z

Gu, Y., Jiang, Z., Ren, D., Shang, Y., Hu, Y., & Yi, L. (2021). Electrochemiluminescence sensor based on the target recognition-induced aggregation of sensing units for Hg^{2+} determination. *Sensors and Actuators B: Chemical, 337*, Article 129821. https://doi.org/10.1016/j.snb.2021.129821

Gu, Y., Li, J., Qian, K., Zhang, Z., Wang, S., & Wang, J. (2020). Integrated dual-signal aptasensor based on magnet-driven operations and miniaturized analytical device for on-site analysis. *Sensors and Actuators B: Chemical, 310*, Article 127856. https://doi.org/10.1016/j.snb.2020.127856

Hernández-Martínez, R., & Navarro-Blasco, I. (2013). Survey of total mercury and arsenic content in infant cereals marketed in Spain and estimated dietary intake. *Food Control, 30*(2), 423–432. https://doi.org/10.1016/j.foodcont.2012.08.016

Kumar, A. (2023). Recent development in fluorescent probes for the detection of Hg^{2+} ions. *Critical Reviews in Analytical Chemistry.*. https://doi.org/10.1080/10408347.2023.2238066

Lan, L., Niu, Q., & Li, T. (2018). A highly selective colorimetric and ratiometric fluorescent probe for instantaneous sensing of Hg^{2+} in water, soil and seafood and its application on test strips. *Analytica Chimica Acta, 1023*, 105–114. https://doi.org/10.1016/j.aca.2018.03.023

Li, H., Huang, X., Mehedi Hassan, M., Zuo, M., Wu, X., Chen, Y., & Chen, Q. (2020). Dual-channel biosensor for Hg^{2+} sensing in food using au@ag/graphene-upconversion nanohybrids as metal-enhanced fluorescence and SERS indicators. *Microchemical Journal, 154*, Article 104563. https://doi.org/10.1016/j.microc.2019.104563

Li, P., Liu, H., Yang, L., & Liu, J. (2013). Sensitive and selective SERS probe for hg(II) detection using aminated ring-close structure of rhodamine 6G. *Talanta, 106*, 381–387. https://doi.org/10.1016/j.talanta.2013.01.013

Luo, L., Xi, C., Zhuo, J., Liu, G., Yang, S., Nian, Y., … Wang, J. (2022). A portable dual-mode colorimetric platform for sensitive detection of Hg^{2+} based on $NiSe_2$ with Hg^{2+}-activated oxidase-like activity. *Biosensors & Bioelectronics, 215*, Article 114519. https://doi.org/10.1016/j.bios.2022.114519

Marsousi, S., Karimi-Sabet, J., Moosavian, M. A., & Amini, Y. (2019). Liquid-liquid extraction of calcium using ionic liquids in spiral microfluidics. *Chemical Engineering Journal, 356*, 492–505. https://doi.org/10.1016/j.cej.2018.09.030

Meng, R., Zhu, Q., Long, T., He, X., Luo, Z., Gu, R., Wang, W., & Xiang, P. (2023). The innovative and accurate detection of heavy metals in foods: A critical review on electrochemical sensors. *Food Control, 150*, Article 109743. https://doi.org/10.1016/j.foodcont.2023.109743

Mhd Haniffa, M. A. C., Ching, Y. C., Illias, H. A., Munawar, K., Ibrahim, S., Nguyen, D. H., & Chuah, C. H. (2021). Cellulose supported promising magnetic sorbents for magnetic solid-phase extraction: A review. *Carbohydrate Polymers, 253*, Article 117245. https://doi.org/10.1016/j.carbpol.2020.117245

Nan, X., Huyan, Y., Li, H., Sun, S., & Xu, Y. (2021). Reaction-based fluorescent probes for Hg^{2+}, Cu^{2+} and Fe^{3+}/Fe^{2+}. *Coordination Chemistry Reviews, 426*, Article 213580. https://doi.org/10.1016/j.ccr.2020.213580

Neng, J., Zhang, Q., & Sun, P. (2020). Application of surface-enhanced Raman spectroscopy in fast detection of toxic and harmful substances in food. *Biosensors and Bioelectronics, 167*, Article 112480. https://doi.org/10.1016/j.bios.2020.112480

Peveler, W. J. (2024). Food for thought: Optical sensor arrays and machine learning for the food and beverage industry. *ACS Sensors, 9*(4), 1656–1665. https://doi.org/10.1021/acssensors.4c00252

Piotrowski, C., Garcia, R., Garrido-Varo, A., Perez-Marin, D., Riccioli, C., & Fearn, T. (2019). Short communication: The potential of portable near infrared spectroscopy for assuring quality and authenticity in the food chain, using Iberian hams as an example. *Animal, 13*(12), 3018–3021. https://doi.org/10.1017/S1751731119002003

Rocío-Bautista, P., Moreno-González, D., Martínez-Piernas, A. B., García-Reyes, J. F., & Molina-Díaz, A. (2022). Novel liquid chromatography/mass spectrometry-based approaches for the determination of glyphosate and related compounds: A review. *Trends in environmental. Analytical Chemistry, 36*, Article e00186. https://doi.org/10.1016/j.teac.2022.e00186

Song, G., Guo, X., Li, Q., Liao, J., Wang, D., Yuan, T., Li, L., Fang, R., Zhang, M., Shen, Q., Zheng, F., & Gong, J. (2023). Simultaneous determination of various heavy metal and arsenic ions in seafood using functionalized fibrous silica (KCC-1) coated stir bar sorptive extraction prior to inductively coupled plasma mass spectrometry. *Food Control, 152*, Article 109846. https://doi.org/10.1016/j.foodcont.2023.109846

Su, G., Yu, C., Liang, S., Wang, W., & Wang, H. (2024). Multi-omics in food safety and authenticity in terms of food components. *Food chemistry, 437*(Pt 2), Article 137943. https://doi.org/10.1016/j.foodchem.2023.137943

Sun, R., Li, Y., Du, T., & Qi, Y. (2023). Recent advances in integrated dual-mode optical sensors for food safety detection. *Trends in Food Science & Technology, 135*, 14–31. https://doi.org/10.1016/j.tifs.2023.03.013

Tang, C., Qiao, J., Wen, Y., Zeng, Z., Shao, S., & Dong, S. (2022). Quality control of woody edible oil: The application of fluorescence spectroscopy and the influencing factors of fluorescence. *Food Control, 142*, Article 109275. https://doi.org/10.1016/j.foodcont.2022.109275

Tsotsou, G. E., & Potiriadi, I. (2022). A UV-vis spectrophotometric methodology for quality control of stevia-based extracts in the food industry. *Food Control, 137*, Article 108932. https://doi.org/10.1016/j.foodcont.2022.108932

Wang, T., Xie, C., You, Q., Tian, X., & Xu, X. (2023). Qualitative and quantitative analysis of four benzimidazole residues in food by surface-enhanced Raman spectroscopy combined with chemometrics. *Food Chemistry, 424*, Article 136479. https://doi.org/10.1016/j.foodchem.2023.136479

Yang, Y., Guo, Y., Jia, X., Zhang, Q., Mao, J., Feng, Y., Yin, D., Zhao, W., Zhang, Y., Ouyang, G., & Zhang, W. (2023). An ultrastable 2D covalent organic framework coating for headspace solid-phase microextraction of organochlorine pesticides in environmental water. *Journal of Hazadous Materials, 452*, Article 131228. https://doi.org/10.1016/j.jhazmat.2023.131228

Yi, L., Wang, W., Diao, Y., Yi, S., Shang, Y., Ren, D., Ge, K., & Gu, Y. (2024). Recent advances of artificial intelligence in quantitative analysis of food quality and safety indicators: A review. *TrAC Trends in Analytical Chemistry, 180*, Article 117499. https://doi.org/10.1016/j.trac.2024.117944

Zamora-Ledezma, C., Negrete-Bolagay, D., Figueroa, F., Zamora-Ledezma, E., Ni, M., Alexis, F., & Guerrero, V. H. (2021). Heavy metal water pollution: A fresh look about hazards, novel and conventional remediation methods. *Environmental Technology & Innovation, 22*, Article 101504. https://doi.org/10.1016/j.eti.2021.101504

Zhang, H., Li, Y., & Gan, F. (2023). Design and fabrication of dual functional sulfur nanodots with reducibility and fluorescence properties for sensitive and selective analysis of metal ions in environmental water samples. *Sensors and Actuators B: Chemical, 374*, Article 132817. https://doi.org/10.1016/j.snb.2022.132817

Zhang, H., Li, Y., Lu, H., & Gan, F. (2022). A ratiometric fluorescence and colorimetric dual-mode sensing platform based on sulfur quantum dots and carbon quantum dots for selective detection of Cu^{2+}. *Analytical and Bioanalytical Chemistry, 414*(7), 2471–2480. https://doi.org/10.1007/s00216-022-03888-w

Zhang, W., Zhong, H., Zhao, P., Shen, A., Li, H., & Liu, X. (2022). Carbon quantum dot fluorescent probes for food safety detection: Progress, opportunities and challenges. *Food Control, 133*, Article 108591. https://doi.org/10.1016/j.foodcont.2021.108591

Zhao, Y., Shi, L., Miao, H., & Jing, X. (2021). "add on" dual-modal optical immunoassay by Plasmonic metal NP-semiconductor composites. *Analytical Chemistry, 93*(6), 3250–3257. https://doi.org/10.1021/acs.analchem.0c04856

Zhu, S., Lou, X., Zhu, J., Song, Z., Hao, Y., Yang, J., & Lu, M. (2024). Ultra-stable Co_3O_4/$NiCo_2O_4$ double-shelled hollow nanocages as headspace solid-phase microextraction coating for enhanced capture of polychlorinated biphenyls. *Chemical Engineering Journal, 488*, Article 150876. https://doi.org/10.1016/j.cej.2024.150876